

# The Single-Particle Spectra of Cuprates

Lijun Zhu, Vivek Aji, Arkady Shekhter and C. M. Varma

Department of Physics and Astronomy, University of California, Riverside, California 92521

The dispersion and linewidth of the entire single-particle spectra for metallic cuprates, irrespective of dopings, measured by angle-resolved photoemission above the superconducting gap and pseudogap, have universal features. The linewidth is linear in frequency up to a scale  $\omega_c$  and is a constant beyond. The cusp in the linewidth at  $\omega_c$  mandates, due to causality, a “waterfall” observed in the dispersion. These features are quantitatively explained by a microscopic theory of quantum-critical fluctuations of a loop-current phase, where the fluctuations are specified by an upper cutoff  $\omega_c$  and a coupling constant to electrons  $\lambda$ . For a given cuprate,  $\lambda$  and  $\omega_c$  varying by less than 20% describe the entire spectra at all measured dopings; from one cuprate to the other the variation required in these parameters is less than 50%.

PACS numbers: 74.20.Mn, 74.25.Jb, 74.72.-h

*Introduction.* With increased refinement of technique and imaginative use, angle-resolved photoemission spectroscopy (ARPES) on the high temperature superconductors has revealed that novel physical principles determine the single-particle spectra in such compounds [1, 2]. Recently, the single-particle spectra over an energy range from the chemical potential to about 1 eV below it have been mapped for several momentum vectors crossing the Fermi surface for various dopings in many different cuprates [3, 4, 5, 6, 7, 8, 9]. In interpreting this data, one must be careful [10] to distinguish between effects arising from ARPES matrix elements from those intrinsic to the spectral function  $A(\mathbf{k}, \omega)$ . We focus in this paper on the recent data from energies above the superconducting gap and the pseudogap to energies of O(1eV) by considering only data which obey Kramers-Kronig(KK) relations so that they are intrinsic to  $A(\mathbf{k}, \omega)$ .

Together with the earlier work [1, 2, 11, 12, 13], the most important results of these recent ARPES experiments can be summarized as follows:

(i) The spectra for energies  $\omega$  in the range of interest are universal; they have the same functional form for all cuprates and for all dopings in the metallic range. Moreover, even the parameters in the functional form vary less than by a factor of 2 over the entire range of cuprates irrespective of whether they are underdoped, optimally doped or overdoped. The data in this energy range is a continuation of the lower energy data for the normal state ( $T > T_c$ ) for near optimal doping [11, 13]. This is best seen in Figs. 1 and 2 of Ref. 3 and similar figures for different compounds and dopings in Refs. 5, 8 and through the analysis which will be presented below.

(ii) The momentum distribution curves (MDC) at constant energy  $\omega$  is a Lorentzian with width  $w_{\mathbf{k}}(\omega)$ . In the energy range of interest  $w_{\mathbf{k}}$  varies linearly with  $\omega$  up to a cutoff above which it is approximately a constant. This is modified if the bare velocity  $\mathbf{v}(\mathbf{k})$  varies within  $w_{\mathbf{k}}$ , which happens as the bottom of the band is approached. See Fig. 3 below for representative experimental data.

(iii) The peak of the MDC as a function of  $\omega$  moves

with  $\mathbf{k}$  defining the renormalized dispersion  $\varepsilon(\mathbf{k})$ . The observed dispersion  $\varepsilon(\mathbf{k})$  follows the band-structure  $\epsilon_{\mathbf{k}}$  with a smooth renormalization factor up to  $\omega \approx E_1$ . Above  $E_1$ , the “velocity”  $d\varepsilon(\mathbf{k})/dk$  sharply increases up to another cutoff  $E_2$  where  $\varepsilon(\mathbf{k})$  resumes the normal dispersion. The nearly vertical dispersion has been picturesquely termed a “waterfall” [3]. In the energy range,  $E_1 \lesssim \omega \lesssim E_2$ , there is also an indication of multiple  $\varepsilon(\mathbf{k})$  for fixed  $\omega$  [6, 8].  $E_1$  varies systematically with the direction of momentum in which the data is taken; it is largest in the  $(\pi, \pi)$  direction and smallest in the  $(\pi, 0)$  direction. Similarly, the position of the “waterfall” in  $\mathbf{k}$ -space varies systematically in the Brillouin zone.

We show that all these features follow quantitatively from the critical fluctuations derived recently [14] whose asymptotic form was proposed phenomenologically earlier [15] and shown to lead to a “marginal Fermi liquid”. These fluctuations, due to a new class of topological charges, are scale-invariant in frequency and local in space. We find that, given the bare band-structure  $\epsilon_{\mathbf{k}}$ , the entire data can be fitted with the two parameters of this theory, a cutoff  $\omega_c$  and a coupling constant  $\lambda$  of the right order of magnitude.

*Single-particle spectral function.* The single-particle spectral function deduced by ARPES is given by the spectral function

$$A(\mathbf{k}, \omega) = -\frac{1}{\pi} \frac{\text{Im}\Sigma(\omega, \mathbf{k})}{[\omega - \text{Re}\Sigma(\omega, \mathbf{k}) - \epsilon_{\mathbf{k}}]^2 + [\text{Im}\Sigma(\omega, \mathbf{k})]^2}. \quad (1)$$

$\Sigma(\omega, \mathbf{k})$  is the self-energy function. The band-structure  $\epsilon_{\mathbf{k}}$  is well-fitted by the tight-binding dispersion

$$\epsilon_{\mathbf{k}} = -2t(\cos k_x a + \cos k_y a) - 4t' \cos k_x a \cos k_y a - 2t''(\cos 2k_x a + \cos 2k_y a) - \mu. \quad (2)$$

The parameters  $t, t', t''$  are given by tight-binding fits to the calculated band-structure [16]. For the high energy range of interest, much larger than the temperatures of measurement, corrections due to finite temperature are unimportant [17]. So the only input from the microscopic

theory is the self-energy  $\Sigma(\omega, \mathbf{k})$  for the extrapolated normal state as  $T \rightarrow 0$ .

*Microscopic Theory.* A microscopic theory for the cuprates [14, 18, 19] is based on the realization, motivated by the phenomenology, that the central organizing feature in the physics of the metallic phase of the cuprates are quantum critical fluctuations of loop currents. In this theory the ordering of these loop currents below  $T_g$  (PG in inset of Fig. 1) leads to a phase which breaks time-reversal symmetry but preserves translational symmetry. Direct evidences for such an ordered state have been obtained by polarized neutron scattering in  $\text{YBa}_2\text{Cu}_3\text{O}_{6+x}$  [20] and by dichroic ARPES experiments in  $\text{Bi}_2\text{Sr}_2\text{CaCu}_2\text{O}_{8+x}$  [21], for various  $x$  in the pseudo-gap phase. The properties in the entire funnel shaped region (I) in inset of Fig. 1 are determined by the quantum critical fluctuations of the loop currents. Therefore universal properties are predicted for  $\omega$  larger than the superconducting gap or the pseudogap for all  $x$  in the metallic phases on either side of  $x_c$ .

The microscopic theory of the fluctuations above the predicted pseudogap phase [14] finds that they have an absorptive part

$$\text{Im}\chi(\mathbf{q}, \nu) = \begin{cases} \chi_0 \tanh \frac{\nu}{2T}, & |\nu| < \omega_c; \\ 0, & |\nu| > \omega_c. \end{cases} \quad (3)$$

$\omega_c$  is a cutoff and  $\chi_0$  gives the integrated weight of the fluctuations. In the microscopic theory [14],  $\omega_c^2 \approx EVR^2$ , where  $E$  is the local repulsion or charging energy parameter,  $V$  the nearest neighbor Cu-O interaction, and  $R$  is the dimensionless loop-current order parameter. For  $E \simeq 10\text{eV}$ ,  $V \simeq 1 - 2\text{eV}$  and  $R \simeq 0.1$ , we expect  $\omega_c \approx 0.3 - 0.5\text{eV}$ . In the entire funnel shaped region under discussion,  $\omega_c$  can have only trivial dependence on  $x$  or  $T$  due to smooth variation of microscopic parameters.

*Calculation of the Self-energy.* The loop current fluctuations at momentum  $\mathbf{q}$  scatter fermions from  $\mathbf{k}$  to  $\mathbf{k} + \mathbf{q}$  with the amplitude  $\gamma(\mathbf{k}, \mathbf{k} + \mathbf{q})$ . From the microscopic model, we find [22]

$$\gamma(\mathbf{k}, \mathbf{k}') = i\frac{V}{2} \left[ \frac{s_x(k+k')}{s_{xy}(k)} + (x \leftrightarrow y) + (k \leftrightarrow k') \right]. \quad (4)$$

Here  $V$  is the nearest neighbor Cu-O repulsion parameter and  $s_{x,y}(k) \equiv \sin(k_{x,y}a/2)$  and  $s_{xy}(k) \equiv \sqrt{s_x^2(k) + s_y^2(k)}$ . The leading self-energy contribution is

$$\Sigma(i\omega_n, \mathbf{k}) = T \sum_{\mathbf{q}, i\nu_n} |\gamma(\mathbf{k}, \mathbf{k} + \mathbf{q})|^2 G(i\omega_n + i\nu_n, \mathbf{k} + \mathbf{q}) \chi(\mathbf{q}, i\nu_n) \quad (5)$$

where  $\omega_n, \nu_n$  are Matsubara frequencies of the quasi-particle and the fluctuating mode, respectively. Given a  $\mathbf{q}$ -independent  $\chi$ , it is straightforward to see that for  $\gamma(\mathbf{k}, \mathbf{k} + \mathbf{q})$  of the form of Eq. (4), the self-energy is independent of  $\mathbf{k}$  for a circular Fermi surface. For a square

Fermi surface, we have estimated that the variation of the self-energy at a given  $\omega$  is about 20% from near the  $(\pi, \pi)$  to the  $(\pi, 0)$  directions. Since the actual Fermi surface for  $x$ 's of interest are closer to a circle than a square, we can ignore this dependence to much better than 20% accuracy.

At zero temperature we get for self-energy

$$\begin{aligned} \text{Im}\Sigma^R(\omega) &= -N(0)\langle\gamma^2\rangle \int_0^\omega \text{Im}\chi^R(\nu) \\ &= -\lambda \frac{\pi}{2} \begin{cases} |\omega|, & |\omega| < \omega_c \\ \omega_c, & |\omega| > \omega_c \end{cases} \\ \text{Re}\Sigma^R(\omega) &= -\frac{\lambda}{2} \left[ \omega \ln \frac{\omega_c}{|\omega|} + (\omega - \omega_c) \ln \frac{|\omega - \omega_c|}{\omega_c} - (\omega \rightarrow -\omega) \right], \end{aligned} \quad (6)$$

where  $N(0)$  is a density of states per one spin species and notation  $\langle\gamma^2\rangle$  stands for average of  $|\gamma(\mathbf{k}, \mathbf{k} + \mathbf{q})|^2$  over the Fermi surface. Here we introduce a dimensionless coupling constant  $\lambda = (2/\pi)N(0)\chi_0\langle\gamma^2\rangle$  which determines coupling between the electrons on the Fermi surface and the loop current fluctuations.

Given a leading order momentum independent self-energy, the vertex corrections [23] to the self-energy are only of  $O(\lambda\omega_c/W)$ , where  $W$  is the bare bandwidth of the conduction band. Using the  $\omega_c$  and  $\lambda$  fitted to the experiments, this ratio is of  $O(0.1)$ . The remaining processes, repeated scattering (self-consistent Born approximation) produces no corrections. At low energies compared to  $\omega_c$ , Eq. (6) reduces to the marginal Fermi liquid form deduced earlier [15].

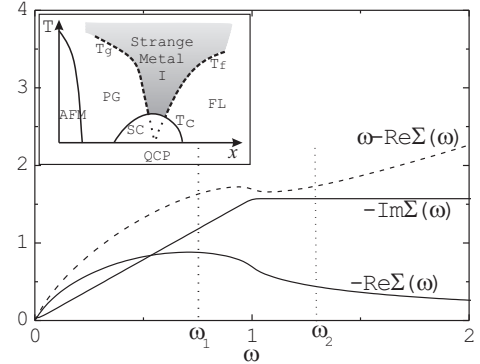


FIG. 1: The real and imaginary parts of the self-energy, and  $\omega - \text{Re}\Sigma(\omega)$  as functions of  $\omega$  for  $\lambda = 1$ . All quantities are dimensionless in units of  $\omega_c$ . The observable dispersion  $\varepsilon(\mathbf{k})$  for a given bare  $\epsilon_{\mathbf{k}}$ , solved by Eq. (7) is equivalent to the intersection of  $\omega - \text{Re}\Sigma(\omega)$  with a horizontal line at  $\epsilon_{\mathbf{k}}$ . As  $\omega - \text{Re}\Sigma(\omega)$  has a wide reentrant region for  $\omega_1 \leq \omega \leq \omega_2$ , the observed dispersion falls from  $\omega_1$  to  $\omega_2$  for a very small variation in  $\epsilon_{\mathbf{k}}$  producing the “waterfall”. Insert shows the phase-diagram of the cuprates; the shaded region shows the region of frequencies and  $x$  under discussion.

The calculated self-energy at  $\lambda = 1$ , and  $\omega_c = 0.41\text{eV}$  (suitable to fit the experimental data [8] in

La<sub>1.83</sub>Sr<sub>0.17</sub>CuO<sub>4</sub>) is shown in Fig. 1. Similar fits are obtained for data [3, 6] for underdoped, optimally doped and overdoped Bi(2212) with  $\lambda \simeq 0.8 \pm 0.1$  and  $\omega_c \simeq 0.5\text{eV}$ , and for [5] an underdoped sample of LBCO with  $\lambda \simeq 1.0$  and  $\omega_c \simeq 0.4\text{eV}$ .

Given the sharp change in the slope in the imaginary part near  $\omega_c$ , the real part has a logarithmic divergence in its slope at  $\omega_c$  before changing from its low energy form  $\propto \omega \log |\omega|$  to  $1/\omega$  for  $\omega \gg \omega_c$ . This sharp variation of  $\text{Re}\Sigma(\omega)$  near  $\omega_c$  is responsible for the observed “waterfall” feature as we now proceed to show. The logarithmic divergence in the slope is smoothened for a smooth upper cutoff; however, we find that a smoothening of the cutoff by a width  $O(\omega_c/10)$  does not affect the comparison with experiments.

*The Waterfall.* The dispersion of the quasi-particles,  $\varepsilon(\mathbf{k})$  given by

$$\varepsilon(\mathbf{k}) - \text{Re}\Sigma(\varepsilon(\mathbf{k})) - \epsilon_{\mathbf{k}} = 0. \quad (7)$$

As shown in Fig. 1,  $\omega - \text{Re}\Sigma(\omega)$  has a wide reentrant region from  $\omega_1 \leq \omega \leq \omega_2$ . The solution of Eq. (7) therefore produces a “waterfall” in the dispersion  $\varepsilon(\mathbf{k})$  because it varies over the large energy range  $\omega_1$  to  $\omega_2$  for a very small variation in  $\mathbf{k}$ . The multiple solutions obtained in this region are within  $\text{Im}\Sigma(\omega)$  for  $\lambda$  of  $O(1)$ . Above  $\omega \simeq \omega_2$ , the dispersion becomes just a renormalized band-structure. The calculated “waterfall” is shown in Fig. 2. The spectral intensity maps in (d),(e),(f) of this figure should be compared with Fig. 1(a),(b),(c) of Ref. [8]. Details are discussed below.

*Universality of the Data.* Now we consider each of the points (i) to (iii) of the experimental data and explain them successively.

(i) The physical properties in any quantum critical regime are universal, controlled by the scale-invariant critical fluctuations. Specifically, for  $\omega$  larger than the superconducting gap or the pseudogap the self-energy is of the marginal Fermi liquid form and given in terms of only the two parameters  $\omega_c, \lambda$  for each compound for all  $x$ . Weak dependences in these parameters from variation in microscopic parameters due to varying  $x$  or  $T$  may of-course occur. We find however that for a given compound, a single value of these parameters is adequate to fit all the data for all  $x$  (underdoped, optimal-doped and overdoped samples), and for all momentum directions.

It is worth noting that the spectra for energies below the pseudogap energy and  $T \leq T_g$  is also scale-invariant with a new scale  $\propto T_g(x)$  [24, 25]. Usually the spectra inside the superconducting dome at low energies is scale-invariant with scale of the superconducting gap. However, for the cuprates, superconductivity in the pseudogap regime might introduce a mixing of the two scales in the spectra.

(ii) Suppose at certain energy  $\omega$ , Eq. (7) is satisfied for  $\mathbf{k} = \mathbf{k}_0$ . If  $\Sigma$  does not depend significantly on  $\mathbf{k}$ , we can expand the spectral function in  $(\mathbf{k} - \mathbf{k}_0)$ . The MDC is

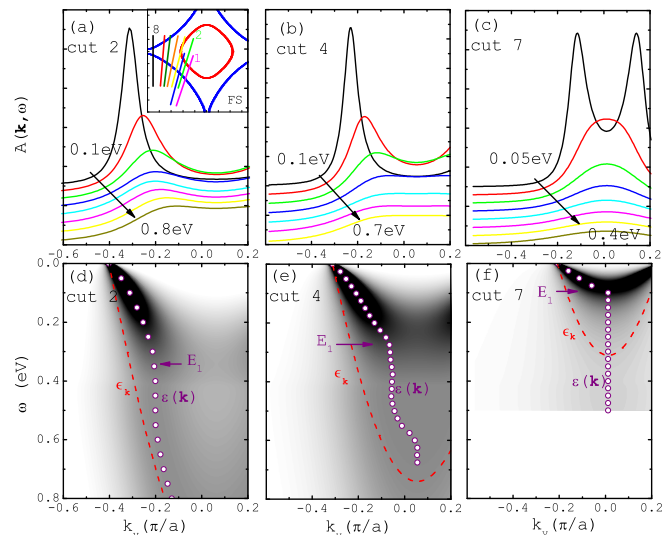


FIG. 2: (a),(b) and (c): Calculated MDC’s for three of the momentum cuts 2, 4 and 7 shown in the inset to Fig. (a) for which data is available from Ref. 8. The MDC’s are shown at various energies  $\omega$  labeled in the figures. Figs. (d),(e) and (f) are spectral intensity maps, for the same cuts respectively. From the intensity maps, we can identify the dispersion  $\varepsilon(\mathbf{k})$  marked by circles; the bare dispersion  $\epsilon_{\mathbf{k}}$  are shown in dashed lines. The inset of Fig. (a) shows the Fermi surface and eight momentum cuts done in experiments [8]. It also shows the position of the “waterfall” in  $\mathbf{k}$ -space for radial cuts with the additional contour drawn inside the Fermi surface.

then a Lorentzian with width  $w_{\mathbf{k}}$  given by  $\text{Im}\Sigma(\omega)/v(\mathbf{k}_0)$  where  $v(\mathbf{k}_0) = v_y(\mathbf{k}_0) + v_x(\mathbf{k}_0)(k_x - k_{x0})/(k_y - k_{y0})$ , is the bare velocity in the direction of interest. This expansion also requires that within  $(\mathbf{k} - \mathbf{k}_0) \approx w_{\mathbf{k}}$ , the velocity  $\mathbf{v}_{\mathbf{k}}$  is nearly a constant.

As discussed above  $\text{Im}\Sigma(\omega)$  increases linearly in  $\omega$  for  $\omega \lesssim \omega_c$  and is constant beyond. Therefore if  $\mathbf{v}_0(\mathbf{k})$  varies slowly with  $\mathbf{k}$  as in cut 2 in Fig. 2, MDC linewidths also vary linearly in  $\omega$ , i.e.,  $w_{\mathbf{k}} \propto \omega$ . Away from the nodal momentum directions,  $\mathbf{v}_0(\mathbf{k})$  varies considerably as in cut 4 and higher of Fig. 2. As a result, MDCs’ half-width taken at half-maximum deviates from the linear- $\omega$  dependence. This accounts for the MDC width of cut 5 shown as an example in Fig. 3 and the higher cuts. If the MDC linewidth is multiplied by the bare velocity at each  $\mathbf{k}$  in any direction, a linear dependence of the width with  $\omega$  is obtained both in theory and the experiments, showing that the self-energy does not depend measurably on the direction in momentum space.

(iii) Comparing Figs. 2(d),(e),(f), we can see that there are two distinct reasons for the “waterfalls”. If  $\epsilon_{\mathbf{k}}$  reaches  $\omega_1 - \text{Re}\Sigma(\omega_1)$  at  $\mathbf{k} \approx \mathbf{k}_0$  as  $\mathbf{k}$  is varied along the momentum cut, e.g., cut 2 in Fig. 2,  $\varepsilon(\mathbf{k})$  follows the “waterfall” between  $\omega_1$  and  $\omega_2$ . However, if the momentum cuts are sufficiently away from the nodal cut such that the bottom of the band is very shallow,  $\epsilon_{\mathbf{k}}$

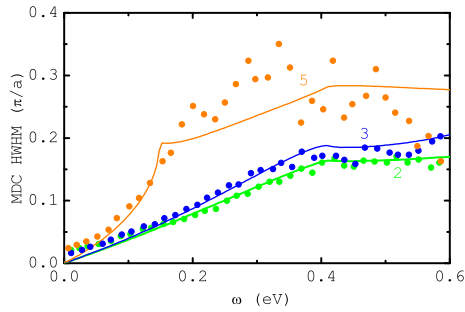


FIG. 3: The MDC half-width  $w_{\mathbf{k}}(\omega)$  is shown for the cuts 2, 3 and 5 of the inset of Fig. 2(a). The experimental data for the same cuts from Fig. 2 of Ref. 8 is also shown. Note that the experiments quote are done with an energy resolution of 30 meV, which accounts for the deviation from the theory at low energies. Higher resolution data [13] confined to lower energies is consistent with the theory. The cusp in the calculated curve for cut 5 at about 0.15 eV (besides the cusp at  $\omega_c \approx 0.4$  eV) is due to the fact that the bottom of the band is reached. The experimental data from near this energy to above is so noisy that KK relation test cannot be applied, see Ref. 10.

never reaches  $\omega_1 - \text{Re}\Sigma(\omega_1)$ ; e.g., cuts 5-8 in Fig. 2. The observed dispersion  $\varepsilon(\mathbf{k})$  then follows Eq. (7) to its maximum value at the bottom of the band  $\mathbf{k}_m$ . For higher energies, there are no solutions to Eq. (7). In this case, let us expand the denominator of Eq. (1) as  $[\mathbf{v}(\mathbf{k}_m)(k_c - k_{cm})]^2 + I(\omega) + [\text{Im}\Sigma(\omega)]^2$ , where  $k_c$  is in the direction of the cut. We see then that the MDC curves stay centered at  $\mathbf{k}_m$  while their linewidths are  $\sqrt{I(\omega) + [\text{Im}\Sigma(\omega)]^2}/v(\mathbf{k}_m)$ . Here  $E_1$  where this type of “waterfall” emerges is less than  $\omega_1$ . Correspondingly, an additional cusp in linewidth is observed at  $E_1$  (e.g., cut 5 in Fig. 3).

It thus follows that the position of the experimentally observed “waterfall”  $E_1$  is nearly equal to  $\omega_1$  for momentum cuts close to the  $(\pi, \pi)$  direction, where the renormalized bandwidth is much larger than  $\omega_1$  and nearly equal to the energy of the bottom of the renormalized band  $\varepsilon(\mathbf{k}_m)$  close to the  $(\pi, 0)$  direction where the renormalized bandwidth is smaller than  $\omega_1$ .

Since, the bottom of the band (where the velocity is zero) becomes continuously more shallow as one moves from the  $(\pi, \pi)$  to the  $(\pi, 0)$  direction,  $E_1$  gets continuously smaller. The variation of the position of the “waterfall”’s, Fig. 3 of Ref. [8] and Fig. 3 of Ref. [6] is thereby completely explained. Similarly the position of the “waterfall” in momentum space is the locus of  $\mathbf{k}$  where  $\varepsilon(\mathbf{k}) \approx E_1$ . This locus is shown in Fig. 2(a) for radial cuts (when  $E_1 \approx \omega_1$ ) and is to be compared with data in Fig. 4 of Ref. [8] and Fig. 4 of Ref. [6]. For cuts in directions far away from the normal to the Fermi surface, the contour gets strongly deformed towards the  $(\pi, 0)$  points.

*Concluding remarks.* The single-particle spectral func-

tion reflects every many body effect which is relevant. Any theory of scattering from fluctuations with a sharp upper cutoff at around 0.4 eV will produce features of the data provided that the coupling to the fermions is strong enough. So, one must ask if features of the experimental results, (i) to (iii), can distinguish among the possible theories. It is possible to do so from the fact that the scattering rate is linear in  $\omega$  up to about  $\omega_c$  and that its coefficient is nearly independent of  $\mathbf{k}$ . We do not know any other ideas proposed for cuprates which have these properties.

All the ARPES results for both linewidth and dispersion have universal properties which are quantitatively explained by the specific theory of quantum critical fluctuations in region I of Fig. 1. The same fluctuations explain the resistivity, optical conductivity, Raman scattering and the anomalous nuclear relaxation rate on Cu in Region I. In fact, no other proposal made explains all these properties. Since superconductivity is an instability of the normal state, only the fluctuations which dominate the properties of the normal state can give rise to pairing. Indeed approximate inversion [26, 27] of ARPES yields that the pairing fluctuations at  $T_c$  have a spectrum consistent with Eq. (3) with a cutoff at about 0.4 eV.

*Acknowledgments.* CMV is especially grateful to Joel Mesot for interesting him in the problem and to him, Johan Chang, Stéphane Paillhès and Christopher Mudry for a detailed discussion of the data. Thanks are also due to Jeff Graf and Alessandra Lanzara for some communications regarding their data.

- 
- [1] J. C. Campuzano, M. R. Norman, and M. Randeria, in *The Physics of Superconductors* Vol. II, ed. K. H. Bennemann and J. B. Ketterson (Springer, Berlin, 2004), p. 167.
  - [2] A. Damascelli, Z. Hussain, and Z.-X. Shen, *Rev. Mod. Phys.* **75**, 473 (2003).
  - [3] J. Graf *et al.*, *Phys. Rev. Lett.* **98**, 067004 (2007); cond-mat/0607319.
  - [4] B. P. Xie *et al.*, cond-mat/0607450.
  - [5] T. Valla *et al.*, cond-mat/0610249.
  - [6] J. Graf, G.-H. Gweon, A. Lanzara, cond-mat/0610313.
  - [7] Z.-H. Pan *et al.*, cond-mat/0610442.
  - [8] J. Chang *et al.*, cond-mat/0610880.
  - [9] W. Meevasana *et al.*, cond-mat/0612541.
  - [10] In D.S. Inosov *et al.*, cond-mat/0703223, it is pointed out quite correctly that the variation of the photoemission matrix elements with momentum can lead to misleading conclusions about the spectral function and produce faux “waterfalls”. This complication is especially severe for data near the center of the Brillouin zone, where the matrix elements nearly vanish. A diagnostic remedy suggested in this paper is that the effects of the matrix elements cannot obey Kramers-Kronig relations. So, correct conclusions about the spectral function may be obtained if the real and imaginary part of the self-energy deduced

from the experiment obeys Kramers-Kronig (KK) relation. This procedure is strictly followed in the present paper by considering only data with cuts across the Brillouin zone, where KK relation is followed. See also the caption to Fig. 3.

- [11] T. Valla *et al.*, Science **285**, 2110 (1999).
- [12] E. Abrahams and C. M. Varma, Proc. Natl. Acad. Sci. USA **97**, 5714 (2000).
- [13] A. Kaminski *et al.*, Phys. Rev. B **71**, 014517 (2005).
- [14] V. Aji and C. M. Varma, cond-mat/0610646.
- [15] C. M. Varma *et al.*, Phys. Rev. Lett. **63**, 1996 (1989).
- [16] Eq. (2) was used in Ref. [8] to fit the Fermi surface of LSCO, with  $t'/t = -0.144$ ,  $t''/t = 0.072$ , and  $\mu/t = -0.84$ . We use the same values with  $t = 0.48eV$  consistent with fits to LDA calculations, see, e.g., R. J. Radtke and M. R. Norman, Phys. Rev. B **50**, 9554 (1994).
- [17] This has been checked through direct evaluation.
- [18] C. M. Varma, Phys. Rev. Lett. **83**, 3538 (1999).
- [19] C. M. Varma, Phys. Rev. B **73**, 155113 (2006).
- [20] B. Fauqué *et al.*, Phys. Rev. Lett. **96**, 197001 (2006).
- [21] A. Kaminski *et al.*, Nature (London) **416**, 610 (2002).
- [22] This is a straightforward extension to  $\mathbf{q} \neq 0$  of the  $\mathbf{q} = 0$  result of Eq. (44) of Ref. [19].
- [23] A. B. Migdal, Zh. Eksp. Teor. Fiz. **34** 1438 (1958) [Sov. Phys. JETP, **7** 996 (1958)].
- [24] A. Kanigel *et al.*, Nature Physics **2**, 447 (2006); cond-mat/0605499.
- [25] C. M. Varma and L. Zhu, cond-mat/0607777; to appear in Phys. Rev. Lett.
- [26] M. Eschrig and M. R. Norman, Phys. Rev. B **67**, 144503 (2003).
- [27] Ref. 26 also find a small (less than 10%) contribution from the 41 meV peak. But since that peak only occurs below  $T_c$ , it can only affect the value of the gap below  $T_c$  and not  $T_c$  itself. The complete development of the pairing spectrum can be deduced through the procedure suggested in I. Vekhter and C. M. Varma, Phys. Rev. Lett. **90**, 237003 (2003).